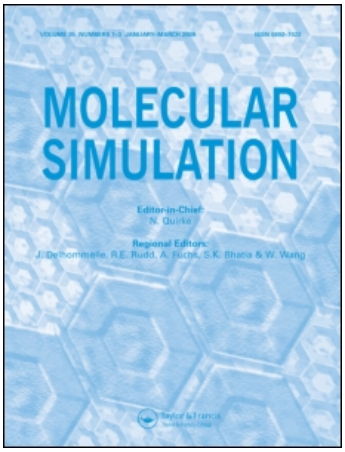

Molecular Simulation
Publication details, including instructions for authors and subscription information:
http://www.informaworld.com/smpp/title~content=t713644482

Viscous drag forces in gas operated pressure balances

V. P. Sokhan[a]; N. Quirke[a]; J. Greenwood[b]
[a] Chemistry Department, Imperial College, London, UK [b] Division of Engineering and Process Control, National Physical Laboratory, Teddington, UK

To cite this Article Sokhan, V. P. , Quirke, N. and Greenwood, J.(2005) 'Viscous drag forces in gas operated pressure balances', Molecular Simulation, 31: 6, 535 — 542
To link to this Article: DOI: 10.1080/08927020500134318
URL: http://dx.doi.org/10.1080/08927020500134318

Molecular Simulation, Vol. 31, Nos. 6–7, 15 May – 30 May 2005, 535–542

Taylor & Francis
Taylor & Francis Group

Viscous drag forces in gas operated pressure balances

V. P. SOKHAN†, N. QUIRKE†* and J. GREENWOOD‡

†Chemistry Department, Imperial College, London SW7 2AY, UK
‡Division of Engineering and Process Control, National Physical Laboratory, Hampton Rd, Teddington TW11 0LW, UK

(Received March 2005; in final form March 2005)

Accurate determination of all forces acting on the piston in the gas operated pressure balance is a long-standing problem in high precision pressure measurements. A major contribution, responsible for the difference between the actual and the effective areas of the piston, is due to the drag force on the piston, and at a fundamental level surprisingly little is known about this force. We present here a first detailed analysis of the hydrodynamics shear forces acting at the gas–piston interface on a molecular level, using effective intermolecular potential functions and a large-scale non-equilibrium molecular dynamics simulation to model the flow of several gases. We show using the hydrodynamic approach that the drag force on the piston for force-driven plane steady-state flow is exactly one half of the external driving force independent of the boundary conditions, justifying a widely accepted assumption in pressure balance theory, and verify this result in computer simulation for a range of gas densities. The natural fall rates using different gases as the pressure transmission medium were measured experimentally for a range of generated pressures and estimated from computer simulation using force-driven Poiseuille flow. Both results, which are in excellent agreement, show pronounced species dependence. This, however, cannot explain the gas species dependence of the effective area.

Keywords: Interfacial friction; Nanoflow; Drag force; Molecular dynamics simulation

1. Introduction

Gas-operated pressure balances are used as primary sources to produce accurate static pressures. With current technology the generated pressure is thought to be reproducible to within several parts per million (ppm). However, a long standing problem in high precision pressure measurements using gas-operated pressure balances is the accurate determination of all forces acting on the piston [1]. Inaccuracies in the calculated force result in device dependent systematic error and may be responsible for observed differences in nominally identical devices of the order of several ppm per MPa. There are several factors responsible for these differences [2] and further progress in the accuracy of pressure calibration requires better understanding of the processes on the fundamental level.

In the piston–cylinder unit (PSU) the gravitational force due to the piston mass and a concentric stack of annular weights acting along the piston axis is balanced by the force exerted by the pressure (in the absolute mode, or pressure difference in the gauge mode) acting on the bottom surface of the piston, and lateral forces acting on the vertical flanks of the piston by the moving gas in the narrow clearance between piston and cylinder bore. There is also a contribution to the vertical force due to mechanical distortion of the piston–cylinder (PC) geometry caused by the pressure gradient and some other contributions of lesser importance [1,3]. While there have been some progress reported recently in estimation of the distortion coefficient [4–7], much less is known about the viscous drag force on the piston. Existing phenomenological models for drag forces [1,8,9] rely on the no-slip viscous flow approximation or use interpolation between viscous flow and molecular flow approximations applicable at low pressures which while they may be appropriate for macroscopic channels are of questionable validity when applied to nanoscale channels ($\sim$200 nm) of the sort used in high pressure gas balances. It has become clear from recent experimental [10] and theoretical [11,12] investigations that fluid flow in nano-channels is characterised by a finite slip whose magnitude depends on the dynamic state [13].

As has been observed by scientists at NIST [8,14,15], there are several phenomena which cannot be explained within the standard theory described in Dadson *et al.* [1]. Thus, there is a dependence of the effective area on the gas

*Corresponding author. E-mail: nickquirke@ic.2c.uk

Molecular Simulation
ISSN 0892-7022 print/ISSN 1029-0435 online © 2005 Taylor & Francis Group Ltd
http://www.tandf.co.uk/journals
DOI: 10.1080/08927020500134318

species used in the calibration; moreover the estimated effective area is different when calibration is made in absolute and in the gauge mode. These phenomena indicate that theory needs to be extended to include the effects of slippage at the wall and rarefaction. Recently, there have been several attempts to improve on the Stokesian model (flow of negligible fluid inertia) and to account for molecular slip at the gas–piston interface [8,16]. Thus, Schmidt *et al.* [8] proposed a phenomenological model for the drag forces on the piston based on the solution of the Navier–Stokes equation in the Poiseuille geometry interpolating between the Knudsen and molecular regimes. However, their model is based on the assumption of a single phase for the gas in the crevice and does not take into account the effects of adsorption. Bergoglio *et al.* [16] used the finite element method to calculate the piston fall rates. From the comparison of estimated and measured fall rates they conclude that slip effects could be important.

In this paper, we present the results of the first realistic simulation of the gas flow in PSU for a range of gases used (Ne, Ar, Kr, N_2) using large-scale non-equilibrium molecular dynamics and calculate for the first time the viscous drag force on the piston directly from the molecular properties. In our simulation we do not include effects of distortion, considered in detail in other publications [4–7]. Instead, we focus on the interfacial friction term, responsible for the drag force in the force balance equation for the floating piston, predict its magnitude and relate it to the material properties of the gas and the piston.

2. Viscous drag force in force-driven flow

In the standard theory of the pressure balance [1], pressure is defined as a force acting on the so-called *effective area* of the piston, S_{eff}, introduced to retain a simple relation between the gravitational force due to the piston mass and all weights and the pressure of the gas (see figure 1). Therefore, S_{eff} is a single unknown property in the problem, which includes effects of geometric distortion of the piston and cylinder and incorporates all (unknown) additional forces acting on the piston. A complex problem of determination of these forces is avoided by postulating the existence of the so-called *neutral surface* at which the viscous friction forces in the fluid disappear [1]. In the generalized case of a position dependent radius of the piston and cylinder the effective area is defined by the following expression,

$$S_{\text{eff}} = \pi r_0^2 \left\{ 1 + \frac{h_0}{r_0} - \frac{1}{r_0(p_1 - p_2)} \int_0^l \mathrm{d}z (p(z) - p_2) \frac{\mathrm{d}(u+U)}{\mathrm{d}z} \right\}. \tag{1}$$

Here, r_0 and h_0 are the undistorted radius and clearance of the piston, u and U are the radial distortions of the piston and cylinder, respectively, and $p(z)$ is the local

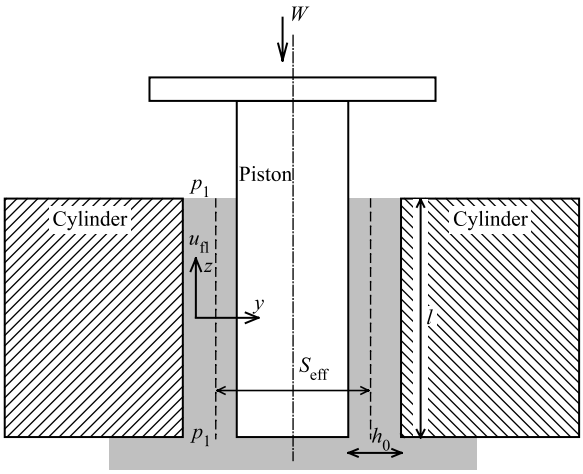

Figure 1. Sketch of the PC assembly.

pressure which varies continuously from the high value p_1 at the bottom of the piston to the ambient pressure p_2 at the top ($p_2 = 0$ in the absolute mode) along the engagement length l. This equation is usually solved for a specified geometric profile in the assumption of a perfect symmetry of rotation of the assembly, and in the linear pressure profile approximation. The second term in braces in equation (1) arises from the neutral surface assumption which is not well founded and indeed confusing; in fact, the argument given on p. 21 of [1] for viscous flow contradicts the fundamental assumptions of the Navier–Stokes hydrodynamics on which it is based. It is easy to show that in the case of force-driven Poiseuille flow the Stokesian hydrodynamics results in a drag force which is independent of the flow conditions, and is related only to the driving force on the system. Thus, for a plane flow along the z direction with walls at $y = \pm h/2$ the average viscous force on a molecule is

$$f(y) = -\nu(y) \frac{\partial^2 u(y)}{\partial y^2}. \tag{2}$$

Here, $\nu(y)$ is a kinematic viscosity ($\nu(y) = \eta/\rho(y)$), $\rho(y)$ is the number density, $u(y)$ is the streaming velocity of the fluid. This frictional force balances the external driving force, f_{g}, which can be of mechanical (gravity) or thermodynamic (chemical potential gradient) origin. Since the number of molecules in a small volume element is simply $\mathrm{d}n = \rho(r)\mathrm{d}x\,\mathrm{d}y\,\mathrm{d}z$, the forces on molecules in the volume are also equal in magnitude and oppositely directed,

$$\begin{aligned} f_{\text{g}}\rho(r)\mathrm{d}x\,\mathrm{d}y\,\mathrm{d}z &= -f(y)\rho(r)\mathrm{d}x\,\mathrm{d}y\,\mathrm{d}z \\ &= \eta \frac{\partial^2 u(y)}{\partial y^2} \mathrm{d}x\,\mathrm{d}y\,\mathrm{d}z, \end{aligned} \tag{3}$$

By integrating equation (3) over the volume of the system between two planes $y = \pm y_0$ in the fluid, we obtain the total driving force, $F_{\text{g}}(y_0) = n_0 f_{\text{g}}$, acting on the n_0 fluid molecules within this slab, and which is balanced

by the viscous force,

$$F_g(y_0) \equiv f_g \int_0^{y_0} dy \rho(y) = A\eta \left. \frac{\partial u(y)}{\partial y} \right|_{y_0}, \quad (4)$$

where $A = L_x L_z$ is the area of the system in xz plane, and the integration constant vanishes by symmetry requirements.[†] We note that in deriving this result it was assumed that the velocity field u and the external force f_g are independent of z, as in the case of gravity-like driven flow. Non-uniform flow with a pressure gradient requires a the knowledge of $u(z)$ or, equivalently, $\rho(z)$. Equation (4), recast in terms of the local shear stress, reads,

$$\Pi_{yz}(y) = A^{-1} F_g(y). \quad (5)$$

This equation illuminates one of the peculiarities of Poiseuille flow: whilst the mean force on the fluid particle is constant, the shear stress increases linearly towards the boundary. The local stress in the fluid at the wall, $y = h/2$, is equal to the drag force on the piston per unit area,

$$\gamma_{dr} \equiv \Pi_{yz}(h/2) = A^{-1} F_g(h/2) \equiv A^{-1} F_{ext}/2 \quad (6)$$

This result shows that for the external force-driven steady-state flow the drag force on the piston is independent of the type of boundary conditions, the total drag force on the solid is equal to the external driving force and therefore for a *plane* Poiseuille flow, the force on *one* wall is equal to half of the driving force. This striking result suggests that the theory of Schmidt *et al.* [8] is incorrect and provides, *for the first time*, a solid foundation for the results obtained in Ref. [1]. Neglecting the distortion of the piston, equation (1) for the effective area of the ideal model of the PC unit reduces to

$$S_{eff} = \pi r_0^2 \left(1 + \frac{h_0}{r_0}\right), \quad (7)$$

and using the notation of Dadson *et al.* [1], the effective area is defined from the equation

$$\begin{aligned} S_{eff}(p_2 - p_1) &= W' + F_{dr} \equiv S(p_2 - p_1) + F_{dr}, \\ &= S(p_2 - p_1) + A_p \gamma_{dr} \\ &= S(p_2 - p_1) + (A_p/A_T) F_{ext} \end{aligned} \quad (8)$$

where S is the physical area of the piston, $F_{dr} = A\gamma_{dr}$ is the drag force on the piston flanks, and $\gamma_{dr} = F_{ext}/A_T$ with $A_T = A_p + A_c$ the sum of the area of the piston and the cylinder, for which we have

$$\frac{A_p}{A_T} \equiv \frac{r_0}{2r_0 + h_0}, \quad (9)$$

Noting that the external force is related to the pressure differential via

$$\begin{aligned} F_{ext} &= \pi(p_2 - p_1)\left((r_0 + h_0)^2 - r_0^2\right) \\ &= \pi(p_2 - p_1)(2r_0 + h_0)h_0, \end{aligned} \quad (10)$$

we obtain

$$S_{eff} = S + \pi r_0 h_0. \quad (11)$$

where the drag force is

$$F_{dr} = \pi r_0 h_0 (p_2 - p_1). \quad (12)$$

Despite the apparent simplicity of this result Schmidt *et al.* [8] arrived at different conclusions (see equation (7) of their paper) and obtained an expression which depends on the shear viscosity of the fluid which, in addition, they assume does not change at the interface (as is shown below, this is a very crude approximation and for the gases studied it overestimates the drag force by two orders of magnitude).

Gas flow in a PC crevice, which is a non-equilibrium process, requires in the general case the solution of the Boltzmann equation. This is a highly non-trivial problem for which there exists, as yet, no solution. A more tractable way forward is to recast the problem within phenomenological hydrodynamics since this approach is computationally efficient and is known to work down to nanometre scale, but this requires the knowledge of bulk material parameters, as well as interfacial parameters entering the boundary conditions, which include now the effects of slippage. An alternative, which provides microscopically detailed information about the flow and conditions at the gas–solid interface, is computer modelling using molecular simulation methods [17], in particular large-scale non-equilibrium molecular dynamics (NEMD) [18]. The controlling parameter is the Knudsen number, defined as a ratio of mean free path to the characteristic length scale (crevice width), $Kn = \lambda/h$. In contrast to oil-operated pressure balances where usually $Kn < 10^{-3}$ and the flow is well approximated by the solution of the incompressible Navier–Stokes equations, in narrow pores of gas operated pressure balances, such as clearances in the PSU, the Knudsen number varies by several orders of magnitude, and the situation is especially acute in absolute mode where the gas is progressively rarefied towards the upper edge of the piston and the applicability of Navier–Stokes hydrodynamics became questionable. In addition, the gas layers adjacent to the solid surface, typically several molecular diameters thick, have modified structural and dynamic properties (shear viscosity) in the strong surface adsorption field. Such effects cannot be handled within classical hydrodynamics [19] and require treatment on a more fundamental level in order to provide suitable interfacial material parameters ("interfacial viscosity", responsible for interfacial friction, or drag force on the piston) required for the solution of hydrodynamic equations. In order to make practical calculations, these parameters need to be known in the same way as in the bulk case, i.e. they should be either tabulated as a function of the thermodynamic state or determined from an *ad hoc* empirical equation.

[†]This can be easily shown by further integrating over y to obtain the solution for the velocity profile, the integration constant will be the only term with odd power in y and therefore should be zero for a parabolic flow which is an even function of y.

3. Simulation method and potential model

The gas flow in the crevice of a PC assembly is a non-equilibrium steady-state process where the driving force is the difference in thermodynamic potential between the piston base (gas at high pressure) and the top of the piston, where gas is at atmospheric or other ambient pressure. A typical apparatus used in the pressure calibrations (Ruska high range 2465) includes a piston with diameter 3.27 mm, which is tightly fitted to a cylinder with average clearance width of 0.2 μm; the engagement length is 22.2 mm and the system operates on 99.999% purity N_2 gas at 293 K. An accurate description of this highly non-uniform system requires certain assumptions concerning the pressure distribution along the engagement length. The development of the dual control volume simulation method [20–22] makes it possible to include all intermediate thermodynamic states in one simulation. It is not feasible, however, to include the whole PC unit at a molecular level, since this will require a number of molecules of the order of Avogadro's number. The required system size can be reduced to manageable dimensions by applying significantly larger density (pressure) gradients and rescaling the obtained results back to the original conditions. Special care should be taken to ensure that the system is still in a linear scaling regime. As a first step and in order to make the task more feasible, we used a different approach. We replaced the thermodynamic driving force (chemical potential gradient) by the equivalent mechanical force, which acts as a uniform external driving (gravity-like) field and make the system uniform along the direction of flow in a state specified by the normal pressure which is equal to the mean external normal pressure in the inhomogeneous case. This technique allows us to simulate a gap of realistic transverse dimensions and also to remove the restriction on the lateral dimensions with the aid of periodic boundary conditions.

The chemical potential gradient is related to pressure gradient via Gibbs–Duhem relation

$$\mathrm{d}p = \rho \mathrm{d}\mu, \tag{13}$$

which, taking into account the linear dependence on ρ, can be written for a finite differential

$$\Delta p = \bar{\rho}\Delta\mu, \tag{14}$$

where $\bar{\rho}$ is the average gas density in the system and the chemical potential difference is replaced by the product of the average force acting on a gas molecule and engagement length of the PC unit. This gives the mean force acting on gas molecules

$$F_g = -\frac{\Delta p}{\bar{\rho}L}. \tag{15}$$

Thus, for the gauge mode 7 MPa pressure calibration (typical experimental conditions) the mean density of nitrogen in the crevice at 293 K assuming the linear density profile along the engagement length, is $1.426\,\mathrm{mol\,l^{-1}}$ [23], which gives the mean driving force on particle $F_g = 2.296 \times 10^{-18}$N. We note that the force calculation using equation (15) is based on the assumption of linear density profile along the direction of flow whereas in fact, it is the chemical potential, which is a non-local functional of the density, scales linearly along the pore length. We believe, however, that the errors due to this approximation are insignificant for the conditions of interest and this assumption will be verified and removed in a subsequent publication.

The transport properties of four different gases flowing in the nanocrevice were calculated using NEMD simulation of the representative part of the PC assembly with the force-driven flow protocol. The system, depicted in figure 2 where the vertical arrow shows the direction of flow and left and right surfaces are the surfaces of the solid, consisted of 2236 gas molecules in a square parallelepiped of dimensions $3.7778 \times 3.52338 \times 200.0\,\mathrm{nm}^3$ ($L_x \times L_y \times L_z$) where the first two dimensions are commensurate with lattice spacing of the (0 0 0 1) WC crystal basal plane and 200 nm is a typical gap width. It represents a small part of the cylindrical crevice of the PC assembly and since the gap width is much smaller than the radius of the piston, the effects of curvature of the surfaces are negligibly small. The system was made effectively infinite in x and z using periodic boundary conditions [17] and the gas was in a thermodynamic state corresponding to the external normal pressure of 3.5 MPa and in contact with a thermostat at 293 K. The surfaces of piston and cylinder are modelled as a perfect crystal WC lattice using three molecular layers of W-terminated tungsten carbide with 182 atoms in each layer. The thermal motion of atoms in the solid is of minor importance for the gas flow [12] and we used an athermal wall model.

All interactions in the simulation are treated in the pair-wise approximation. The total potential energy is

$$U = \sum_{j>i} U_{\mathrm{ff}}(r_{ij}) + \sum_{i,j} U_{\mathrm{sf}}(r_{ij}) \tag{16}$$

where U_{ff} and U_{sf} are the fluid–fluid and solid–fluid van der Waals (vdW) potentials, respectively; both of the Lennard–Jones (LJ) form,

$$U(r_{ij}) = 4\varepsilon\left[\left(\frac{\sigma}{r_{ij}}\right)^{12} - \left(\frac{\sigma}{r_{ij}}\right)^{6}\right]. \tag{17}$$

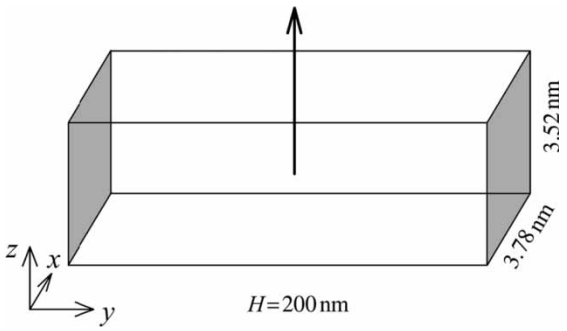

Figure 2. Sketch of the simulation box. In y direction the system is bounded by two plane walls at $y = \pm 100$ nm. The driving force and the gas flow are in z-direction, and the system is periodically replicated in x and z directions.

Table 1. vdW parameters.

	M/u	$\varepsilon/kJ\,mol^{-1}$	σ/nm	*Reference*
W	183.85	2.116	0.278	WLCARB parameter set (http://server.ccl.net/cca/data/METMOD1/carbenes)
C	12.00	0.2328	0.340	A. Vernov, W. A. Steele, *Langmuir*, **8**, 155 (1992)
N_2[†]	28.014	0.4465	0.329	K. Kaneko, R. F. Cracknell, D. Nicholson, *Langmuir*, **10**, 4606 (1994)
Ne	20.18	0.3201	0.2786	Estimated from the critical parameters (T and ρ) fitting. They are slightly different from determined from second virial coefficients (J.O. Hirschfelder, C.F. Curtiss, and R.B. Bird. Molecular Theory of Gases and Liquids, p. 165 (Wiley, NY) 1954.)
Ar	39.95	0.9957	0.3405	
Kr	83.80	1.3295	0.3639	
Xe	131.29	1.8358	0.3957	

[†]Modelled as single LJ site.

Here, ε and σ are empirical material parameters, and their values for the gases studied are collected in table 1. Gas–solid interactions are also described in the model using a set of LJ parameters for the solid atoms. We note that while for the adsorption of nitrogen on tungsten clusters there is a degree of chemisorption [24], there is no such evidence in the case of a tungsten carbide surface. In the simulation we used the standard parameters for the carbon, $\varepsilon/k = 28$ K and $\sigma = 0.34$ nm, and the WCLCARB [25] parameters for tungsten, $\varepsilon/k = 254.5$ K and $\sigma = 0.278$ nm. Potential parameters for the nitrogen, modelled as a single LJ site, were taken from Kaneko *et al.* [26]. All cross-parameters were derived from the corresponding LJ self interactions using the standard combining rules ($\varepsilon_{12} = \sqrt{\varepsilon_{11}\varepsilon_{22}}$, $\sigma_{12} = (\sigma_{11} + \sigma_{22})/2$) [27]. In calculating intermolecular interactions a single cut-off distance of 1.05 nm has been used without further long-range corrections (with this cut-off the long-range correction for pressure in a uniform system of the same density is of the order of 1%). With the potential parameters used here the adsorption energy of nitrogen is 7.1 kJ mol^{-1}.

Each simulation run started from a random configuration of the gas and the equations of motion were solved with a 10 fs time step using the Verlet leap-frog algorithm [17]. All heat produced in the system by the work of the external force, was removed via an efficient Gaussian constraint thermostat [17] which was applied to all degrees of freedom of the gas molecules. In the direction of flow it was applied to the peculiar velocities. At the beginning of each simulation run, the system was in a transient non-equilibrium state and the establishment of a steady-state flow required an initial equilibration stage which was not included in the statistical averages. This initial process in some cases took up to 1 ns of the simulation time. This was followed by a production run with a typical integration time of several microseconds.

Since the drag force exerted by the flowing gas on the piston surface is proportional to the surface area, it is helpful to introduce an intensive quantity, the force per unit area (with units of pressure),

$$\gamma_{\mathrm{fr}} = \frac{F_{\mathrm{fr}}}{S}, \tag{18}$$

which is system independent. It was calculated directly in the course of NEMD simulation,

$$\gamma_{\mathrm{fr}} = L_x^{-1} L_z^{-1} \sum_{i,j} \frac{(z_i - z_j)}{r_{ij}} \frac{\partial U_{\mathrm{sf}}(r_{ij})}{\partial r_{ij}}, \tag{19}$$

where i labels solid atoms and j atoms in the gas. Used together with the appropriate constitutive relation,

$$\Pi_{yz}(y) = -\eta(y) \frac{\partial u_z(y)}{\partial y}, \tag{20}$$

where $\eta(y)$ is a local shear viscosity, we obtain

$$\gamma_{\mathrm{fr}} \equiv \Pi_{yz}(y)\big|_{y=y_{\mathrm{w}}} = -\eta_{\mathrm{sf}} \frac{u_{\mathrm{w}}}{\delta}, \tag{21}$$

where y_{w} is the position of the solid wall, u_{w} is the slip velocity, and δ is the slip length.

4. Results

4.1. NEMD simulation of plane Poiseuille flow: viscous drag force

In order to compare and verify the results of computer simulation against experimental results the following procedure was adopted. All gas molecules were subject to an external uniform gravity-like conservative force taken to be about 100 times the value obtained using equation (15) in order to get observable gas fluxes within NEMD and to reduce the statistical noise. The precise values of the force are given in table 2. Obtained fluxes and fall rates were rescaled linearly down to the forces obtained from equation (15). The forces used in the current work are typical for NEMD simulations, but as an additional check that the generated fluxes are within the linear scaling in the case of nitrogen two additional simulations was performed, one with the force two times smaller, and another with the force

Table 2. Viscous drag force on the piston flanks.

	Ne	*Ar*	*Kr*	N_2
$0.5F_{\mathrm{ext}}$/pN	0.21568	0.42696	0.44782	0.29941
F_{dr}/pN	0.216(2)	0.425(2)	0.448(3)	0.298(2)
F_{Sch}/pN	21.11	42.3	85.9	22.96
f_{fr}/aN	0.207	0.189	0.386	1.17
f_{g}/aN	0.2678	0.1929	0.3819	1.2551

enhanced by 30%. The resulting fluxes were found to scale linearly with force to within statistical uncertainty. The viscous drag force on the piston is the lateral force induced by the moving gas and it is non-zero even for flow with no-slip boundary conditions since even the 'immobilized' molecular layer transfers the momentum of the moving molecules on the gap side to the solid. In this case it is of the same nature as stresses in the solid. This force can be directly calculated in the computer experiment. The values of the drag force on one wall, given in the second row of the table 2, agree well with the corresponding applied forces for all gases. The figures in brackets are the errors (one standard deviation) in the last digit of the quoted numbers. Note that very long runs (several microseconds of laboratory time or several hundred million timesteps of integration) are required in order to obtain the drag force with such precision. The third row in the table presents the drag force obtained using assumptions made in the Schmidt paper [9],

$$F_{\mathrm{Sch}} = A\eta \left.\frac{\partial u(y)}{\partial y}\right|_{y=h/2}, \tag{22}$$

where we used experimental shear viscosities [23] and calculated the derivative from the quadratic fit to simulated profiles. It is clear from the results that the theory of Schmidt *et al.* does not work in case of strong adsorption, as for the WC wall. Using the same viscosities, we estimated the viscous friction force on fluid particles from

$$f_{\mathrm{fr}} = \frac{\eta}{\rho}\frac{\partial^2 u(y)}{\partial y^2}, \tag{23}$$

and compared the values obtained with the external force, the results are given by the two last rows in the table. The agreement is good given the approximations made, and reflects the accuracy of the potential models used in simulation in reproducing the shear viscosity of real gases.

Streaming velocity profiles obtained for four gases and rescaled to an external force of 2.296×10^{-16} N are compared in figure 3. There are two reasons for differences in profiles: the first is the difference in the shear viscosity of the gases, the second is the difference in slip velocity, which results in a shift of the whole distribution. The largest slip velocity appears to be for neon and the smallest is for krypton, monotonically decreasing with the increase in strength of the solid–fluid interactions.

To better understand the details of dissipative forces at the interface we have calculated the different contributions to the mean force experienced by a gas molecule as a function of the distance from the wall. The force balance conditions require that under steady-state viscous flow the total average force on a fluid molecule is zero; therefore all dissipative forces should sum to the driving force with opposite sign, which is constant in our model. It is convenient to define three different shearing force contributions; one is the sum of pair forces for fluid particles "on the left", i.e. over all j particles for which $y_j < y_i$, a second contribution from all particles with $y_j > y_i$, and finally the contribution from the solid–fluid interactions. The profiles for three contributions are shown in figure 4 for the case of nitrogen flow together with the corresponding density profile. The profiles are shown with respect to the solid interface at $y = 0$. As a consequence of the strong adsorption, the solid–fluid friction force is the dominant contribution but it is a very short-ranged force. It decays exponentially and at a distance from the wall equal to one molecular diameter it becomes negligible comparing to fluid-fluid friction. The difference between the left and right fluid forces is the shearing force, which scales approximately linearly with the distance from the middle of the pore. Within the Navier–Stokes hydrodynamics the sum of all friction forces is equal in

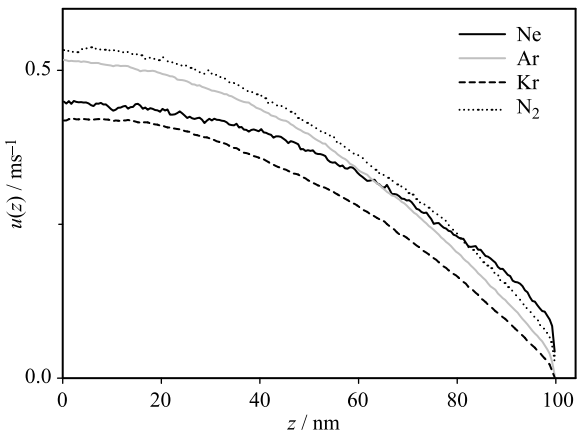

Figure 3. Gas flow velocity profiles across the PC gap for several gases. The surface of the piston and cylinder are at $z = \pm 100$ nm. The system is symmetric with respect to $y = 0$ plane and for clarity only positive half of the profiles is shown.

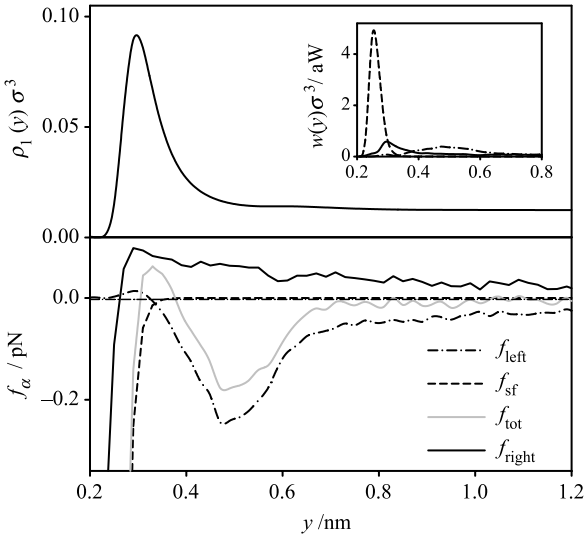

Figure 4. The density profile and different components of the shearing force, acting on the gas molecule as a function of distance from the wall (see text). For comparison, the external driving force is shown with a thin dashed line. The grey line denotes total average force acting on a molecule and is a sum of all contributions including external force. On the inset to the upper graph a power dissipation density profile is shown resolved in components.

magnitude but is of opposite sign to the driving force, shown on figure with a thin dashed line. The sum of all frictional forces, shown on figure with a grey line, indeed fluctuates around the driving force value, however, at the interface, both components of the shearing force deviate from the macroscopically predicted linear dependence as a result of the strong variation of the local density profile in this region. The mean net force on the particle, calculated as the sum of all contributions, including the external driving force, deviates from zero at the interface and there are two regions, one where the particles are accelerated on average, and another where they are decelerated. This striking phenomenon lies outside the hydrodynamic description. Particles in one region experience a macroscopic accelerating field and when they leave this region, they lose the velocity gained in the 'deceleration zone'. The steady-state conditions are maintained therefore due to constant particle circulation between two regions and constant intake of slow particles in the acceleration region. The net acceleration averaged over both regions is of course zero.

The product of the shearing force and local flux defines the dissipation power density,

$$w(y) = |f_{\mathrm{fr}}(y) \cdot u(y)|\rho_1(y), \tag{24}$$

and on the inset to the shearing force graph (figure 4) the dissipation power profile, resolved into three components, is shown. Clearly, the main channel for the energy dissipation is the fluid-wall collision process. Apart from the boundary layer of molecular dimensions, the flow, however, is viscous and the standard laws of hydrodynamics are applicable.

4.2. Experimental validation: fall rate estimation

The fall rate experiments were performed on Ruska 2465 high range gas piston (s/n V-832) using two gases, nitrogen and krypton at 293 K. The fall rate has been determined using the standard technique of cross-floating. The floating piston height was monitored optically using a laser triangulation system, and the fall rate estimated from a linear fit to the temporal profile of the piston height. For each gas the experiments were carried out at three calibration pressures, 0.35283, 0.70377 and 1.40559 MPa in the gauge mode of operation. At each pressure the estimated fall rate was averaged over five independent measurements. The results are shown in figure 5 by symbols together with the corresponding error bars (one standard deviation). Even with this limited data it is clear that the fall rate scales linearly with pressure and that the flow is within the viscous regime. The linear fit, shown with dashed lines, does not pass through the origin and the initial offset is approximately the same for nitrogen and krypton. This indicates that at lower pressures the dependence is non-linear as a result of rarefaction and a transition to the Knudsen regime.

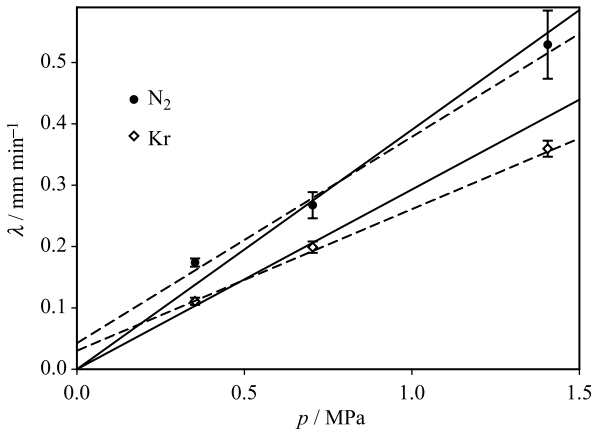

Figure 5. Comparison of the calculated and measured fall rates of for several gases. Symbols, experimental results; lines—calculated from molecular dynamics values scaled linearly with pressure.

From the balance conditions at the piston base, the fall rate λ can be related to the gas velocity u_0 at the crevice entry via

$$\lambda = \frac{2hu_0}{r_0}, \tag{25}$$

where r_0 is the piston radius and h is the mean clearance. Assuming linearity of the density profile along the engagement length and taking into account that the flux is constant along this length, the mean velocity u of the gas is $u = 2u_0$. This gives a relationship between the fall rate and the streaming velocity, calculated in molecular simulation,

$$\lambda_{\mathrm{sim}} = \frac{hu}{r_0}. \tag{26}$$

Using this expression the fall rates were estimated for several gases and the results are shown in figure 5 by solid lines. They are collected in table 3, scaled to the higher calibrated pressure. Taking into account the approximations made, the agreement between simulated and experimental results is excellent. From the gases studied Kr has the lowest fall rate and should give smaller variance in the calibrated pressure.

5. Conclusion

The typical conditions of pressure calibration using gas operated pressure balances correspond to the so-called slip regime, which is a transition regime between viscous and free molecular flow and is characterised by Knudsen numbers $Kn > 0.01$, indicating that the effects of

Table 3. Comparison of the calculated and experimentally measured fall rates for the range of gases scaled to 1.4 MPa calibration pressure

	Ne	*Ar*	*Kr*	N_2
λ_{sim}/mm min^{-1}	0.4824	0.5074	0.4102	0.5466
λ_{exp}/mm min^{-1}	–	–	0.3595	0.5292

rarefaction became perceptible. The good agreement between estimated and measured fall rates, or equivalently, between experimental and simulated fluxes demonstrate that the gas flow in this range still can be described by hydrodynamics with appropriately modified boundary conditions. We show that within the hydrodynamic approach the drag force on the piston for force-driven plane steady-state flow is exactly one half of the external driving force, independent of the boundary conditions, justifying the widely accepted assumption in pressure balance theory of a species independent effective area. Such an assumption is contradicted, however, by the published experimental data of Ehrlich and colleagues [8,14,15] and a growing body of unpublished data collected at NPL. Our simulations, based on the uniform force-driven flow, cannot explain the apparent gas species dependence of the effective area but do provide the basis for further work to elucidate this problem [28].

Acknowledgements

This work is supported by the Strategic Research Program of the National Physical Laboratory, Teddington, UK and the National Measurement System Program in Mass Related Metrology. We thank Mr S. Martimer for the experimental data.

References

[1] R.S. Dadson, S.L. Lewis, G.N. Peggs. *The Pressure Balance. Theory and Practice*, HMSO, London (1982).
[2] C. Ehrlich. A review of gas-operated piston gauges. *Metrologia*, **30**, 585–590 (1993/94).
[3] G.F. Molinar. An old instrument in the new technological scenery: The piston gauge in liquid media up to 1GPa. *Metrologia*, **30**, 615 (1993).
[4] G. Buonanno, M. Dell'Isola, G. Iagulli. A finite element method to evaluate the pressure distortion coefficient in pressure balances. *High Temp. High Press.*, **31**, 131 (1999).
[5] W. Sabuga. Determination of elastic properties of piston gauges using the strain gauge method. Proc. 17 Internat. Conf. on Force, Mass, Torque and Pressure Measurements, IMEKO TC3, Istanbul (2001).
[6] S.Y. Woo, Y.J. Lee, I.M. Choi, B.S. Kim. How to reduce non-linearity in effective area caused by the O-ring seal in a high-pressure balance. *Metrologia*, **39**, 537 (2002).
[7] G. Buonanno, M. Dell'Isola. Design and metrological characterisation of different pressure balances using the finite-element method. *High Temp. High Press.*, **33**, 189 (2001).
[8] J.W. Schmidt, B.E. Welch, C.D. Ehrlich. Operational mode and gas species effects on rotational drag in pneumatic dead weight pressure gauges. *Meas. Sci. Technol.*, **4**, 26–34 (1993).
[9] J.W. Schmidt, S.A. Tison, C.D. Ehrlich. Model for the drag force in the crevice of piston gauges in the viscous-flow and molecule-flow regimes. *Metrologia*, **36**, 565–570 (1999).
[10] H. Hervet, L. Leger. Flow with slip at the wall: from simple to complex fluids. *C.R. Phys.*, **4**, 241–249 (2003).
[11] J.-L. Barrat, L. Bocquet. Large slip effect at a nonwetting fluid–solid interface. *Phys. Rev. Lett.*, **82**, 4671–4674 (1999).
[12] V.P. Sokhan, D. Nicholson, N. Quirke. Fluid flow in nanopores: An examination of hydrodynamic boundary conditions. *J. Chem. Phys.*, **115**, 3878 (2001).
[13] P.A. Thompson, S.M. Troian. A general boundary condition for liquid flow at solid surfaces. *Nature*, **389**, 360–362 (1997).
[14] B.E. Welch, R.E. Edsinger, V.E. Bean, C.D. Ehrlich. Observations of gas species and mode of operation effects on effective areas of gas-operated piston gauges. In *High Pressure Metrology*, G.F. Molinar (Ed.), Vol. 89, p. 81, Bureau International des Poids et Measures Monographie (1989).
[15] J.W. Schmidt, B.E. Welch, C.D. Ehrlich. Gas and mode, vertical and rotational effects with a three piston gauge apparatus. *Metrologia*, **30**, 599–602 (1993).
[16] M. Bergoglio, G. Molinar, N. Antonietti. Piston fall rate in pressure balances: Improvements of the Stokes model. *Acta Metrologica Sinica*, Proceedings of the International Symposium on Pressure and Vacuum 14 (2003).
[17] M.P. Allen, D.J. Tildesley. *Computer Simulations of Liquids*, Clarendon Press, Oxford (1986).
[18] D.J. Evans, G.P. Morriss. *Statistical Mechanics of Nonequilibrium Liquids*, Academic Press, London (1990).
[19] K.P. Travis, B.D. Todd, D.J. Evans. Departure from Navier–Stokes hydrodynamics in confined liquids. *Phys. Rev. E*, **55**, 4288 (1997).
[20] G.S. Heffelfinger, F. van Swol. Diffusion in Lennard–Jones fluids using dual control volume grand canonical molecular dynamics simulation (DCV-GCMD). *J. Chem. Phys.*, **100**, 7548 (1994).
[21] J.M.D. MacElroy. Nonequilibrium molecular dynamics simulation of diffusion and flow in thin microporous membranes. *J. Chem. Phys.*, **101**, 5274 (1994).
[22] R.F. Cracknell, D. Nicholson, N. Quirke. Direct molecular dynamics simulation of flow down a chemical potential gradient in a slit-shaped micropore. *Phys. Rev. Lett.*, **74**, 2463–2466 (1995).
[23] B.A. Younglove. Thermophysical properties of fluids: Part 1. *J. Phys. Chem. Ref. Data*, **11**(Suppl. 1), 619 (1985) *erratum* **14**, 619 (1982).
[24] S.A. Mitchell, D.M. Rayner, T. Bartlett, P.A. Hackett. Reaction of tungsten clusters with molecular nitrogen. *J. Chem. Phys.*, **104**, 4012 (1996).
[25] WLCARB parameter set (http://server.ccl.net/cca/data/METMOD1/carbenes)
[26] K. Kaneko, R.F. Cracknell, D. Nicholson. Nitrogen adsorption in slit pores at ambient temperatures: Comparison of simulation and experiment. *Langmuir*, **10**, 4606 (1994).
[27] J.O. Hirschfelder, C.F. Curtiss, R.B. Bird. *Molecular Theory of Gases and Liquids*, Wiley, NY (1954).
[28] V.P. Sokhan, N. Quirke (work in progress).